Supplement to Z. Phys. D - Atoms, Molecules and Clusters 21, S 23-27 (1991)

Atoms, Molecules and Clusters
Zeitschrift für Physik D

Electron scattering theory for highly charged ions

M. S. Pindzola and N. R. Badnell
Department of Physics, Auburn University, Auburn, Alabama, USA

D. L. Moores
Department of Physics and Astronomy, University College London, London, UK

D. C. Griffin
Department of Physics, Rollins College, Winter Park, Florida, USA

Abstract

Lowest-order QED theory using distorted wave states provides a convenient description for many electron scattering processes involving highly charged atomic ions. We apply QED theory to calculate ionization, excitation, and dielectronic recombination cross sections for electron scattering from highly charged uranium ions. For ionization and dielectronic recombination we compare theory with recent heavy ion accelerator measurements. We also apply lowest-order electroweak gauge theory using distorted wave states to examine the Z-scaling of parity-violating neutral current contributions to the KLL Auger decay of atomic ions.

I. Introduction

Electron scattering processes involving highly charged ions provide information on the quantum mechanical dynamics of few-body relativistic systems under a known force law. Dynamical information so gleaned may then prove useful in studies of other relativistic systems, like quarks inside hadrons[1], for which the force laws are more complicated. Lowest-order QED theory[2] provides a convenient description for many electron-ion scattering processes. For near threshold ionization and excitation cross sections, as well as dielectronic recombination cross sections, the use of plane wave states in QED is no longer valid. In this paper we first review the application of distorted wave theory to the calculation of the lowest-order Feynman diagrams for electron-ion scattering[3]. We then apply QED theory using distorted-wave states to calculate ionization, excitation, and dielectronic recombination cross sections for electron scattering from highly charged uranium ions. For ionization and dielectronic recombination we compare theory with recent heavy ion accelerator measurements[4],[5]. As a challenge to future heavy ion accelerator and storage ring experiments, we apply electroweak gauge theory[6] using distorted wave states to calculate parity-violating neutral current contributions to the KLL Auger decay of uranium ions.

II. Theory

The electron-impact ionization cross section may be derived starting with the two Feynman diagrams shown in Fig. 1. The direct scattering amplitude (in atomic units) is given by[2]

$$S_d = i\int d^4x \int d^4y \int d^4q \; \frac{1}{(2\pi)^4} \; \bar{\psi}_f(x)\gamma_u\psi_i(x) \; \frac{e^{-iq(x-y)}}{q^2 + i\alpha} \; \bar{\psi}_e(y)\gamma^u\psi_b(y) \; , \quad (1)$$

while the exchange scattering amplitude is given by

$$S_e = -i\int d^4x \int d^4y \int d^4q \; \frac{1}{(2\pi)^4} \; \bar{\psi}_e(x)\gamma_u\psi_i(x) \; \frac{e^{-iq(x-y)}}{q^2 + i\alpha} \; \bar{\psi}_f(y)\gamma^u\psi_b(y) \; , \quad (2)$$

where the γ_u are 4x4 matrices, q is the 4 momentum transfer, and the Lorentz gauge has been chosen for the photon propagator. The

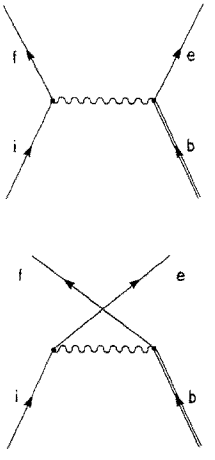

Fig. 1 Lowest-order Feynman diagrams for electron scattering with a bound state electron (double line).

Dirac bispinor wavefunctions, $\psi(x)$, are labeled as to the target bound state and the incident, final, and ejected scattering states. The 12 dimensional integrals found in Eqs. (1) and (2) may be reduced to 2 dimensional radial integrals through the introduction of partial wave expansions for the incident, final, and ejected wavefunctions, as well as the photon propagator.

For an electron ionization process of the form:

$$e^- + (n_b\ell_b j_b)^w \rightarrow (n_b\ell_b j_b)^{w-1} + 2e^- \quad , \qquad (3)$$

where w is the occupation number of the relativistic subconfiguration $(n\ell j)$, the subconfiguration-average ionization cross section is given by[3]

$$\sigma_i = \int_o^{E/2} d\varepsilon_e \; \frac{16w}{p_i^3 p_e p_f} \sum_{\ell_i j_i} \sum_{\ell_f j_f} \sum_{\ell_e j_e} [j_i, j_e, j_f] |V|^2_{avg} \quad , \qquad (4)$$

where ε is the total energy of the electron minus its rest energy, $E = \varepsilon_e + \varepsilon_f$, the linear momentum $p = (2\varepsilon + \varepsilon^2/c^2)^{1/2}$, c is the speed of light, and the notation $[j] = 2j + 1$ is used.

The average of the square of the interaction matrix element found in Eq. (4) is given by[3]

$$|V|^2_{avg} = \sum_{\lambda,\lambda',L} (-1)^{\lambda+\lambda'} [j_i, j_f, j_e, j_b]^{-1} \times \left\{ \frac{F(\lambda,L)F^*(\lambda',L) + G(\lambda,L)G^*(\lambda',L)}{[L]} + 2 \sum_{L'} \begin{Bmatrix} j_f & j_i & L \\ j_e & j_b & L' \end{Bmatrix} \text{Real } F(\lambda,L)G^*(\lambda',L') \right\}, \qquad (5)$$

where the standard notation is used for the 6j symbol and the "natural" phase approximation has been chosen. The direct multipole function is given by[3]

$$F(\lambda,L) = R_\lambda(fe;ib)\delta_{\lambda,L}\langle\kappa_f||C^{(\lambda)}||\kappa_i\rangle\langle\kappa_e||C^{(\lambda)}||\kappa_b\rangle + \sum_{\{a_f a_i a_e a_b\}} g(a_f a_i a_e a_b) \, S_\lambda^{a_f a_i a_e a_b}(fe;ib) \, \delta(1\lambda L)\langle a_f\kappa_f||V^{(L)}||a_i\kappa_i\rangle\langle a_e\kappa_e||V^{(L)}||a_b\kappa_b\rangle, \qquad (6)$$

where the set $\{a_f a_i a_e a_b\}$ is summed over (+-+-), (+--+), (-++-), (-+-+), and g = -1,+1,+1,-1 for each of the 4 cases respectively. In Eq. (6), $\langle\kappa_1||C^{(\lambda)}||\kappa_2\rangle$ and $\langle a_1\kappa_1||V^{(L)}||a_2\kappa_2\rangle$ are previously defined[3] reduced matrix elements of tensor operators and $\kappa = -2(j-\ell)(j + 1/2)$. After the interchange $f \leftrightarrow e$, the exchange multipole function, G(λ,L), has the same form as F(λ,L). The 2d retarded static integral is given by

$$R_\lambda(fe;ib) = \int_o^\infty dr \int_o^\infty dr' (2\lambda+1)\xi j_\lambda(\xi r_<) h_\lambda^+(\xi r_>) \times (P_f(r)P_i(r) + Q_f(r)Q_i(r)) (P_e(r')P_b(r') + Q_e(r')Q_b(r')), \qquad (7)$$

and the 2d retarded magnetic integral is given by

$$S_\lambda^{a_f a_i a_e a_b}(fe;ib) = \int_o^\infty dr \int_o^\infty dr' (2\lambda+1)\xi j_\lambda(\xi r_<) h_\lambda^+(\xi r_>) F_{a_f}(r)F_{a_i}(r)F_{a_e}(r')F_{a_b}(r') \quad , \qquad (8)$$

where $j_\lambda(x)$ and $h_\lambda^+(x)$ are spherical Bessel functions, $\xi = (\varepsilon_f - \varepsilon_i)/c$, $F_{a_i}(r) = P_i(r)$ if $a_i = +$, and $F_{a_i}(r) = Q_i(r)$ if $a_i = -$. The continuum radial orbitals found in the 2d integrals of Eqs. (7) and (8) are solutions to the single-channel Dirac equation

$$\left(\frac{d}{dr} + \frac{\kappa}{r}\right) P_{\varepsilon\kappa}(r) + \frac{1}{c}\left[V_n(r) - \varepsilon - 2c^2 + V_{DF}\right] Q_{\varepsilon\kappa}(r) = 0 \; ,$$

$$\left(\frac{d}{dr} - \frac{\kappa}{r}\right) Q_{\varepsilon\kappa}(r) - \frac{1}{c}\left[V_n(r) - \varepsilon + V_{DF}\right] P_{\varepsilon\kappa}(r) = 0 \; , \qquad (9)$$

where $V_n(r)$ is the nuclear potential, the distorting potential operator V_{DF} is constructed from previously calculated Dirac-Fock target orbitals, and the continuum normalization is $(1 + \varepsilon/2c^2)^{1/2}$ times a sine function.

For an electron excitation process of the form:

$$e^- + (n_1\ell_1 j_1)^{w_1}(n_2\ell_2 j_2)^{w_2} \rightarrow (n_1\ell_1 j_1)^{w_1-1}(n_2\ell_2 j_2)^{w_2+1} + e^- \quad , \qquad (10)$$

the subconfiguration-average excitation cross section is given by

$$\sigma_x = \frac{8\pi \, w_1(2j_2 + 1 - w_2)}{p_i^3 p_f} \sum_{\ell_i, j_i} \sum_{\ell_f, j_f} [j_i, j_f] \, |V|^2_{avg} \quad , \qquad (11)$$

where the substitutions b→1 and e→2 are made in the evaluation of $|V|^2_{avg}$ from Eq. (5).

By the principle of detailed balancing, the dielectronic capture cross section is related to the corresponding autoionization rate. For an autoionization process of the form:

$$(n_1\ell_1 j_1)^{w_1}(n_2\ell_2 j_2)^{w_2} \rightarrow (n_1\ell_1 j_1)^{w_1+1}(n_2\ell_2 j_2)^{w_2-2} + e^- \quad , \qquad (12)$$

the subconfiguration-average Auger rate is given by[3]

$$A_a = \frac{4}{p_f} \; \frac{(2j_1+1-w_1)w_2(w_2-1)(2j_2+1)}{4j_2} \sum_{\ell_f, j_f} [j_f] \, |V|^2_{avg} \quad , \qquad (13)$$

where the substitutions i→2, b→2, and e→1 are made in the evaluation of $|V|^2_{avg}$ from Eq. (5). For an autoionization process of the form:

$$(n_1\ell_1 j_1)^{w_1}(n_2\ell_2 j_2)^{w_2}(n_3\ell_3 j_3)^{w_3} \rightarrow (n_1\ell_1 j_1)^{w_1+1}(n_2\ell_2 j_2)^{w_2-1}(n_3\ell_3 j_3)^{w_3-1} + e^- \quad , \qquad (14)$$

the subconfiguration-average Auger rate is given by

$$A_a = \frac{4}{p_f} (2j_1+1-w_1) w_2 w_3 \sum_{\ell_f j_f} [j_f] |V|^2_{avg} , \quad (15)$$

where the substitutions i→3, b→2, and e→1 are made in the evaluation of $|V|^2_{avg}$ from Eq. (5). The dielectronic recombination cross section is obtained by multiplying the dielectronic capture cross section by the branching ratio for radiative stabilization.

Beyond the subconfiguration-average approximation, more detailed level specific cross sections including electron correlation effects may be calculated using the multiconfiguration Dirac-Fock (MCDF) approximation for atomic structures[7]. In the last few years the MCDF method has been successively applied to the calculation of dielectronic recombination cross sections and rate coefficients for many atomic ions[8-10]. In particular Chen has extended the MCDF method to include the Breit interaction and has found significant effects on Auger transitions of highly charged ions[11]. The MCDF method has also been applied to the calculation of electron-impact excitation[12-17] and ionization[18] cross sections for atomic ions.

Electron-impact scattering cross sections may also be derived starting with the two Feynman diagrams of Fig. 1 where the wavy line represents the exchange of the heavy Z_o boson instead of the photon[6]. The direct scattering amplitude is given by

$$\bar{S}_d = \frac{i}{4\sin^2\theta} \int d^4x \int d^4y \int d^4q \frac{1}{(2\pi)^4} \bar{\psi}_f(x)\gamma_u(c_V - c_A\gamma^5)\psi_i(x) \frac{e^{-iq(x-y)}}{q^2 - M^2c^2} \bar{\psi}_e(y)\gamma^u(c_V - c_A\gamma^5)\psi_b(y) , \quad (16)$$

while the exchange scattering amplitude is given by

$$\bar{S}_e = \frac{-i}{4\sin^2\theta} \int d^4x \int d^4y \int d^4q \frac{1}{(2\pi)^4} \bar{\psi}_e(x)\gamma_u(c_V - c_A\gamma^5)\psi_i(x) \frac{e^{-iq(x-y)}}{q^2 - M^2c^2} \bar{\psi}_f(y)\gamma^u(c_V - c_A\gamma^5)\psi_b(y) , \quad (17)$$

where $c_V = -1/2 + 2\sin^2\theta$, $C_A = -1/2$, M is the Z_o mass, and θ is the Weinberg angle. For energies relevant in atomic collisions ($q^2 << M^2c^2$), the Z_o boson propagator can be approximated as a 4 dimensional delta function. The 12 dimensional integrals found in Eqs. (16) and (17) may be reduced to a 1 dimensional radial integral through the introduction of partial wave expansions for the incident, final, and ejected wavefunctions, as well as the delta function.

Parity violating neutral current contributions to electron-ion scattering processes may be cast in almost the same form for the subconfiguration-average cross sections as derived in the preceeding paragraphs for the electromagnetic interaction. The average of the square of the interaction matrix element of Eq. (5) is now given by

$$\left\{|V|^2_{avg}\right\}_{PV} = \left(\frac{c_V c_A}{4\sin^2\theta M^2c^2} \right)^2 \left\{|V|^2_{avg}\right\}_{EM} , \quad (18)$$

where the $1/M^4$ factor guarantees small cross sections. The forms of the multipole functions found in Eq. (5) are also different. The direct multipole function is now given by

$$F(\lambda,L) = \sum_{\{a_f a_i a_e a_b\}} g(a_f a_i a_e a_b)\, T_\lambda^{a_f a_i a_e a_b}(feib) \times \left(\delta_{\lambda,L} \langle a_f\kappa_f||C^{(\lambda)}||a_i\kappa_i\rangle\langle a_e\kappa_e||C^{(\lambda)}||a_b\kappa_b\rangle + \delta(1\lambda L)\langle a_f\kappa_f||V^{(L)}||a_i\kappa_i\rangle\langle a_e\kappa_e||V^{(L)}||a_b\kappa_b\rangle\right) , \quad (19)$$

where the set $\{a_f a_i a_e a_b\}$ is summed over (+++−), (++−+), (−−+−), (−−−+), (+−++), (+−−−), (−+++), (−+−−) and g = +1,−1,+1,−1,+1,+1,−1,−1 for each of the 8 cases respectively. After the interchange f ↔ e, the exchange multipole function, G(λ,L), has the same form as F(λ,L). The odd number of like sign a's in any set for Eq. (19) guarantees an opposite parity selection rule from the even number of like sign a's found in Eq. (6). The 1d radial integral is given by

$$T_\lambda^{a_f a_i a_e a_b}(feib) = \int_o^\infty \frac{dr}{r^2} (2\lambda+1) F_{a_f}(r) F_{a_i}(r) F_{a_e}(r) F_{a_b}(r) . \quad (20)$$

III. Uranium Ion Results

To illustrate the application of lowest order QED theory using distorted wave states, we calculate various cross sections for electron scattering from highly charged uranium ions using the expressions found in the previous section. The near threshold electron-impact ionization cross section for U^{91+} is shown in Fig. 2.[3] The subconfiguration-average cross section calculation (solid curve) is obtained using the σ_i cross section expression of Eq. (4) and the direct term only of $|V|^2_{avg}$ from Eq. (5). As such the calculation contains contributions from the electrostatic, electromagnetic, and retardation parts of the full covariant two-body interaction. For comparison electrostatic only results are presented using both relativistic (dashed curve) and non-relativistic (dotted curve) wavefunctions. The QED distorted wave results (solid curve) agree to 10% with the QED plane-wave calculations of Scofield[19] (dot-dashed curve) at the higher energies. The plane-wave results for U^{91+} continue a steady rise with incident energy to a value of 11.6 barns at 1 GeV. This steady rise in the K shell ionization

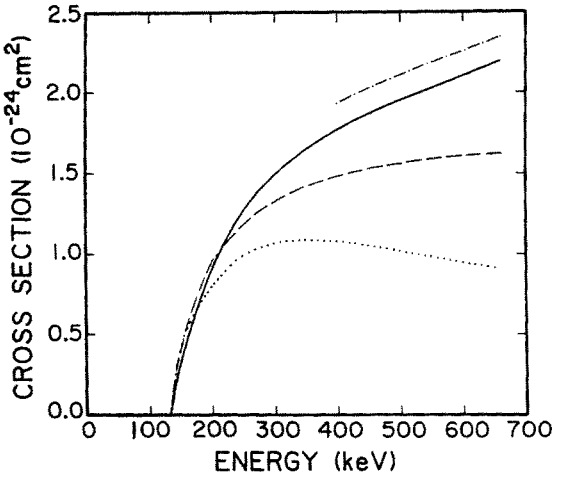

Fig. 2 Electron-impact ionization cross section for U^{91+}. Solid curve, QED theory; dashed curve, Dirac theory; dotted curve, Coulomb theory; dot-dashed curve, plane-wave theory of Scofield (Ref. 19).

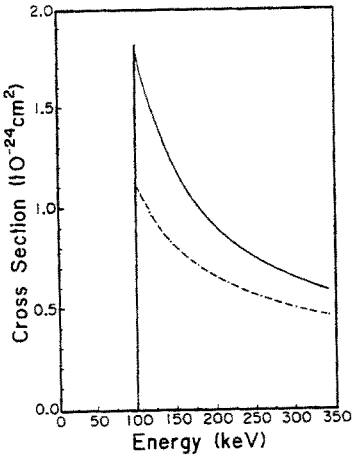

Fig. 3 Electron-impact excitation cross section for the 1s→2s transition in U^{91+}. Solid curve, QED theory; dashed curve, Dirac theory.

cross section has been confirmed experimentally using high-energy electron beams on fixed atomic targets[20]. In the threshold region at 222 keV, recent heavy-ion channeling experiments[4] report a cross section value of 3.9 barns for U^{91+}, with an uncertainty in the measurement giving a range of values from 1.9 barns to 7.8 barns. The QED distorted wave calculation shown in Fig. 1 gives a value of 1.1 barns at 222 keV. Recently we have repeated our QED distorted wave calculations for the electron-impact ionization of U^{91+} including the direct, exchange, and interference terms of $|V|^2_{avg}$ from Eq. (5) and have obtained a value of 1.6 barns at 222 keV.

The near threshold electron-impact excitation cross section for the 1s→2s transition in U^{91+} is shown in Fig. 3. The subconfiguration-average cross section calculation (solid curve) is obtained using the σ_x cross section expression of Eq. (11) and the full expression for $|V|^2_{avg}$ from Eq. (5). For comparison electrostatic only results (dashed curve) are presented using relativistic wavefunctions. We thus observe a 60% increase in the threshold excitation cross section due to the electromagnetic and retardation parts of the full covariant two-body interaction. We have also calculated excitation cross sections for the $1s\rightarrow2\bar{p}(j = 1/2)$ and $1s\rightarrow2p(j = 3/2)$ transitions in U^{91+} and have found increases of 22% and 12% respectively at threshold.

Auger rates for the decay of the lowest autoionizing subconfigurations of U^{89+} are given in Table I. The subconfiguration-average (SCA) results are obtained using the A_a autoionizing rate expressions of Eqs. (13) and (15) and the full expression for $|V|^2_{avg}$ from Eq. (5). The multiconfiguration Dirac Fock-Breit (DFB) results are obtained using methods previously developed[10]. The DFB results are level specific and based on configuration mixing within the even parity subconfigurations ($1s^22s + 1s2s^2 + 1s2\bar{p}^2 + 1s2\bar{p}2p + 1s2p^2$) and within the odd parity subconfigurations ($1s^22\bar{p} + 1s^22p + 1s2s2\bar{p} + 1s2s2p$). For those subconfigurations with more than one level, the DFB result is the (2J+1) weighted average over the allowed levels. The SCA results are obtained using exactly the same DFB orbitals, but of course configuration mixing is ignored. The difference in the rates found in Table I between the two methods can be largely attributed to correlation effects; for example the $1s2s^2$ and $1s2\bar{p}^2$ mix strongly due to their relatively small energy separation.

Table I: U^{89+} Autoionizing Rates

Subconfiguration	Energy (Ry)	SCA Rate (Hz)	DFB Rate (Hz)
$1s2s^2$	4635	5.64(14)	6.26(14)
$1s2s\bar{p}$	4644	2.66(14)	2.75(14)
$1s2\bar{p}^2$	4663	3.85(13)	2.25(12)
1s2s2p	4962	5.12(13)	5.28(13)
$1s2\bar{p}2p$	4975	8.47(13)	7.73(13)
$1s2p^2$	5294	4.74(13)	4.47(13)

The dielectronic recombination cross section for U^{90+} in the energy range encompassing the lowest autoionizing levels of U^{89+} is shown in Fig. 4[10]. Since the radiative rate for highly charged ions is much greater than the autoionizing rate for most doubly excited levels, the dielectronic recombination cross section approximately equals the dielectronic capture cross section which in turn is directly proportional to the various Auger rates. The dielectronic recombination cross section shown in Fig. 4 has been folded with the Compton profile for H_2 and thus represents the resonant transfer excitation (RTEX) cross section for $U^{90+} + H_2$ collisions in the rest frame of the

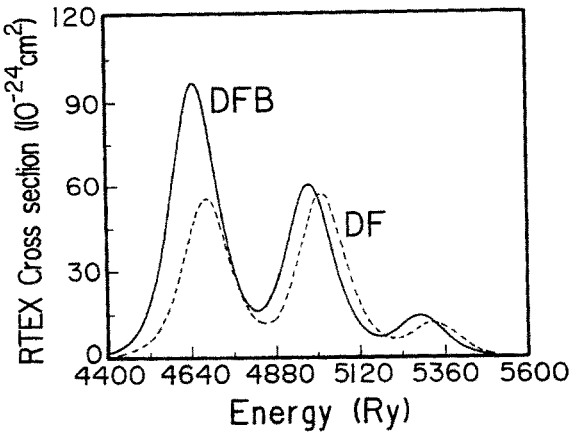

Fig. 4 RTEX Cross Section for U^{90+} collisions with H_2 as a function of projectile energy times m/M. Solid curve: Dirac-Fock method with Breit interaction corrections; dashed curve: Dirac-Fock method.

projectile. The multiconfiguration Dirac-Fock Breit (DFB) results differ substantially from the multiconfiguration Dirac-Fock (DF) results only for the lowest energy peak involving the Auger decay of the $1s2s^2$, $1s2s2\bar{p}$, and $1s2\bar{p}^2$ subconfigurations. Recent heavy-ion accelerator measurements[5] have confirmed both the three peak nature of the U^{90+} cross section and the enhancement of the lower energy peak due to the Breit interaction.

Parity conserving and parity violating Auger rates for the decay of the $2s^2$ (j = 0) state of U^{90+} are given in Table II. Both subconfiguration-average (SCA) results are obtained using the A_a autoionizing rate expression of Eq. (13) and the full expression for $|V|^2_{avg}$ from Eq. (5);

Table II: U^{90+} Autoionizing Rates

Subconfiguration	Energy (keV)	Parity Conserving SCA Rate (Hz)	Parity Violating SCA Rate (Hz)
$2s^2$	64.035	1.18(15)	3.04(-9)

except that the parity violating rate has the substitutions found in Eqs. (18) and (19). The parity conserving rate involves the even parity $1s\varepsilon s$ (j = 0) continuum, while the parity violating rate takes place through the odd parity $1s\varepsilon\bar{p}$ (j = 0) continuum. Based on other similar calculations, the parity violating Auger rate to fill a K shell hole in a singly charged ion scales roughly as Z^8, where Z is the atomic number. Work is in progress to find suitable candidates for analysis by high resolution angle dependent Auger spectroscopy.

IV. Summary

In conclusion lowest order QED theory employing distorted wave states may be applied to a wide range of electron-ion scattering processes. Electromagnetic and retardation corrections to the electrostatic two-body Coulomb interaction are found to be quite significant for highly charged ions. With further development of electron scattering experiments involving heavy-ion accelerators and storage rings it may be possible to not only provide accurate checks on QED theory for strong fields, but on other gauge theory forces as well.

Acknowledgments

This work was supported in part by the Office of Fusion Energy, U.S. Department of Energy, under Contract No. DE-FG05-86-ER53217 with Auburn University and in part by Lawrence Livermore National Laboratory under subcontract No. 8063670 with Auburn University.

References

1. F.E. Close, Proceedings of the 1989 Computational Atomic and Nuclear Physics Summer School (World Scientific, NY, 1990).
2. J.D. Bjorken and S.D. Drell, Relativistic Quantum Mechanics (McGraw-Hill, New York, 1964).
3. M.S. Pindzola, D.L. Moores, and D.C. Griffin, Phys. Rev. A40, 4941 (1989).
4. N. Claytor, B. Feinberg, H. Gould, C.E. Bemis, Jr., J. Gomez del Campo, C.A. Ludemann, and C.R. Vane, Phys. Rev. Lett. 61, 2081 (1988).
5. W.G. Graham, K.H. Berkner, E.M. Bernstein, M.W. Clark, B. Feinberg, M.A. McMahan, T.J. Morgan, W. Rathbun, A.S. Schlachter, and J.A. Tanis, Phys. Rev. Lett, submitted 1990.
6. C. Quigg, Gauge Theories of the Strong, Weak, and Electromagnetic Interactions, (Benjamin/Cummings, Reading, Mass., 1983).
7. I.P. Grant, Advan. Phys. 19, 747 (1970).
8. S. Dalhed, J. Nilsen, and P. Hagelstein, Phys. Rev. A33, 264 (1986).
9. M.H. Chen, Phys. Rev. A33, 994 (1986).
10. M.S. Pindzola and N.R. Badnell, Phys. Rev. A, submitted 1990.
11. M.H. Chen, Nucl. Instr. Methods in Phys. Res. B43, 366 (1989).
12. G.D. Carse and D.W. Walker, J. Phys. B6, 2529 (1973).
13. P.H. Norrington and I.P. Grant, J. Phys. B14, L261 (1981) and J. Phys. B20, 4869 (1987).
14. P.L. Hagelstein and R.K. Jung, At. Data and Nuc. Data Tables 37, 121 (1987).
15. K.J. Reed, M.H. Chen, and A.U. Hazi, Phys. Rev. A36, 3117 (1987).
16. W.J. Qian, Y.K. Kim, and J.P. Desclaux, Phys. Rev. A39, 4509 (1989).
17. H.L. Zhang, D.H. Sampson, and A.K. Mohanty, Phys. Rev. A40, 616 (1989).
18. D.L. Moores and M.S. Pindzola, Phys. Rev. A, submitted 1990.
19. J.H. Scofield, Phys. Rev. A18, 963 (1978).
20. B.L. Moiseiwitsch, Adv. At. and Mol. Phys. 16, 281 (1980).